Structural transition, dielectric and bonding properties of $BeCN_2$*

Gou Hui-Yang(缑慧阳), Gao Fa-Ming(高发明)†,
Zhang Jing-Wu(张静武), and Li Zhi-Ping(李志平)

Department of Chemical Engineering, State Key Laboratory of Metastable Materials Science and Technology, Yanshan University, Qinhuangdao 066004, China

(Received 21 May 2010; revised manuscript received 27 July 2010)

By means of first principle total energy calculations, this paper studies the structural transition, elastic, mechanical, dielectric and electronic properties of $BeCN_2$. The calculations in total energy indicate that under ambient condition, the orthorhombic $BeSiN_2$-type $BeCN_2$ (space group $Pna2_1$) is a more favoured structure than the tetragonal chalcopyrite-type one (space group I-42d). The results of elastic properties reveal that $BeCN_2$ in both orthorhombic and tetragonal structure has higher bulk and shear moduli and smaller Poisson's ratio. The calculated Vicker hardness of tetragonal phase is 36.8 GPa, indicating a hard material. The analyses of electronic structure and electron density difference demonstrate that these excellent mechanical properties are attributed to the stronger covalent-bonding of CN_4 and BeN_4 subunits in $BeCN_2$ crystal. Also, the orthorhombic $BeCN_2$ phase is found to be a transparent semiconductor material with the calculated direct band gap of about 5.56 eV, superior to the indirect band gap of diamond and c-BN. Moreover, it also calculates Born effective charges and dielectric constants of $BeCN_2$. These results suggest that $BeCN_2$ may have some useful applications as optoelectronic, optical window and wear resistant materials.

Keywords: first-principle electron theory, dielectric, bonding
PACS: 62.20.–x, 71.20.–b **DOI:** 10.1088/1674-1056/20/1/016201

1. Introduction

Ternary II–IV-N_2 semiconductors have attracted particular attentions because of their potential applications as optoelectronic materials and even as excellent hosts for ferromagnetic semiconductors by alloy doping.[1−3] The II–IV-N_2 compounds being derived from III-N compounds, where the group-III element is derived from the group-II element (Be, Mg, Zn, etc.) and group-IV element (C, Si, Ge, etc.), are also of great interest as buffer layer for the growth of III-N compounds.[4−15] A large number of experimental and theoretical works focus on the synthesis and understanding the structural, mechanical, electronic, optical, vibrational and dielectric properties of ABN_2 (A=Mg, Zn etc., B=Si, Ge etc.) semiconductors.[4−15] For ternary beryllium nitride, only $BeSiN_2$ phase with orthorhombic structure (space group $Pna2_1$) has been synthesised.[16] By means of *ab initio* calculations, Shaposhnikov *et al.*[17] have studied the electronic and optical properties of $BeSiN_2$ compound with orthorhombic and tetragonal structure. Romer *et al.*[18] studied the pressure-induced structural transition of $BeSiN_2$. For $BeCN_2$, no experimental work has been done due to the toxicity of beryllium compounds. Using first-principle calculation, Lambrecht and Segall[19] have calculated the bulk modulus and electronic structure of $BeCN_2$ with chalcopyrite (space group I-42d) structure. They found that the tetragonal $BeCN_2$ phase has direct band gap. The $BeCN_2$ has been suggested as a candidate for a useful hard material. In this paper, we carried out the detailed calculations on the structural transition, elastic, dielectric and electronic properties of $BeCN_2$ by using first-principle techniques. The Vickers hardness of $BeCN_2$ has been predicted based on Mulliken overlap population in first-principles technique. It was found that $BeCN_2$ in both orthorhombic and tetragonal structure is in the elastically and thermodynamically stable phase and there exists a pressure-induced phase transition from orthorhombic to tetragonal structure. The calculated electronic properties indicate that both the orthorhombic and tetragonal $BeCN_2$ phases are direct wide band gap materials, and the tetragonal $BeCN_2$ possesses the excellent mechanical properties.

*Project supported by the National Natural Science Foundation of China (Grant No. 50672080).
†Corresponding author. E-mail: fmgao@ysu.edu.cn
© 2011 Chinese Physical Society and IOP Publishing Ltd

2. Details and calculations

To carry out the first-principles calculations, we consider two different crystal structures for $BeCN_2$: (i) the orthorhombic $BeSiN_2$-type structure (space group $Pna2_1$, No. 33), which is related to the wurtzite structure and contains four formula units and each N is tetrahedrally surrounded by two Be and two X atoms;[16,19] (ii) the tetragonal chalcopyrite structure (space group I-42d, No. 142), which originates from the zinc blende structures and has four formula units in each unit cell and each atom is tetrahedrally coordinated to four neighbouring atoms.[4−20] In these structures, the tetrahedral units by sharing four corners form three-dimensional networks. However the stacking sequences of the nitrogen atoms are different.[21,22]

All the present calculations have been carried out by using CASTEP code[23] based on the density functional theory (DFT). The exchange and correlation functional was treated by the local density approximation (LDA-CAPZ).[24] The Vanderbilt ultrasoft pseudo-potential[25] was used with cutoff energy of 350 eV for $BeCN_2$ in both orthorhombic and tetragonal structures, k-points of 9×9×9 are generated by using the Monkhorst–Pack scheme.[26] The convergence tolerances for geometrical optimisation were set as the maximum energy change within 5×10^{-6} eV/atom, the maximum ionic Hellmann–Feynman force within 0.01 eV/Å, the maximum ionic displacement within 5×10^{-4} Å (1 Å=0.1 nm), and the maximum stress within 0.02 GPa. Mulliken overlap populations[27] were integrated by a distance cutoff of 3 Å. Moreover, the phonon frequencies of $BeCN_2$ are subsequently obtained by using the linear response method as implemented in the CASTEP code, the norm-conserving pseudo-potential[28] with the energy cutoff of 770 eV was employed for all the considered structures. The lattice dynamics and dielectric properties are calculated within the framework of density functional perturbation theory (DFPT). Technical details of the calculations can be found in Refs. [23] and [29].

3. Results and discussion

The equilibrium lattice parameters, obtained by performing total-energy calculations, are shown in Table 1 for $BeCN_2$ in both orthorhombic and tetragonal structures. The lattice parameters (a and c) of tetragonal $BeCN_2$ phases are consistent with the previous theoretical results.[19,20] From Table 1, we know that b/a and c/a ratio of orthorhombic $BeCN_2$ phase are 1.21 and 0.97 with LDA, respectively, which are much smaller than the expected value of 1.732 and 1.633 respectively.[13] While for $BeCN_2$ in tetragonal structure, c/a ratio, 1.84 with LDA, is also slightly deviated from the ideal chalcopyrite value, 2.0.[19,20] Furthermore, the total energy differences (ΔE_0) per formula unit between the orthorhombic and tetragonal phases of $BeCN_2$ are also given in Table 1. The total energy of the orthorhombic $BeCN_2$ is lower than that of the tetragonal one, indicating that the orthorhombic phase of $BeCN_2$ is energetically the more favourable structure at ground state. Which is similar to the other ternary nitrides, ABN_2 (A=Be, Mg, Zn, Cd; B=Si, Ge, Sn).[13,21] Also, between these two phases, the difference of $BeCN_2$ in energy and density with generalised-gradient approximation (GGA), 18 meV and 0.6%, respectively, are higher than that of $BeSiN_2$ (5 meV and 0.3%, respectively).[18] Moreover, the calculated total energy as a function of the volume for $BeCN_2$ with GGA is given in Fig. 1(a). It shows that a phase transition may occur between the orthorhombic and tetragonal phases under ambient conditions. To accurately obtain the structural transition pressure, we calculate the enthalpy difference (ΔH) of $BeCN_2$ relative to the orthorhombic structure as a function of pressure displayed in the inset of Fig. 1(a) with GGA. It is found that the orthorhombic structure is stable up to 21 GPa and then transforms to the tetragonal structure. This transition pressure is slightly higher than that of $BeSiN_2$, 20 GPa,[22] which is consistent with the trend of the difference of total energy. The structural transition path between orthorhombic and tetragonal structures is shown in Fig. 1(b). Upon compression along the [120] direction, the sliding and shuttle of atoms in the nitrogen tetrahedron of the orthorhombic structure result in the tetragonal structure. As the atoms gradually move from their original position under compression, the highly distorted tetrahedron in the orthorhombic structure is reduced, this fact makes the structure more symmetrical. After overcoming the small energy barrier, the tetragonal configuration is easy to form for $BeCN_2$ because there is only bond alteration in length without breaking any bonds across the structural transition.

Table 1. Calculated equilibrium lattice parameters, a_0/Å, b_0/Å, c_0/Å, total energy difference ΔE_0 (meV/$BeCN_2$).

$BeCN_2$			a	b	c	ρ	ΔE_0
$Pna2_1$	LDA	This work	4.373	5.278	4.224	3.345	0
	GGA	This work	4.424	5.329	4.269	3.236	0
I-42d	LDA	This work	3.746		6.904	3.365	11
		Theor.[20]	3.71		7.272		
	GGA	This work	3.782		6.994	3.256	18

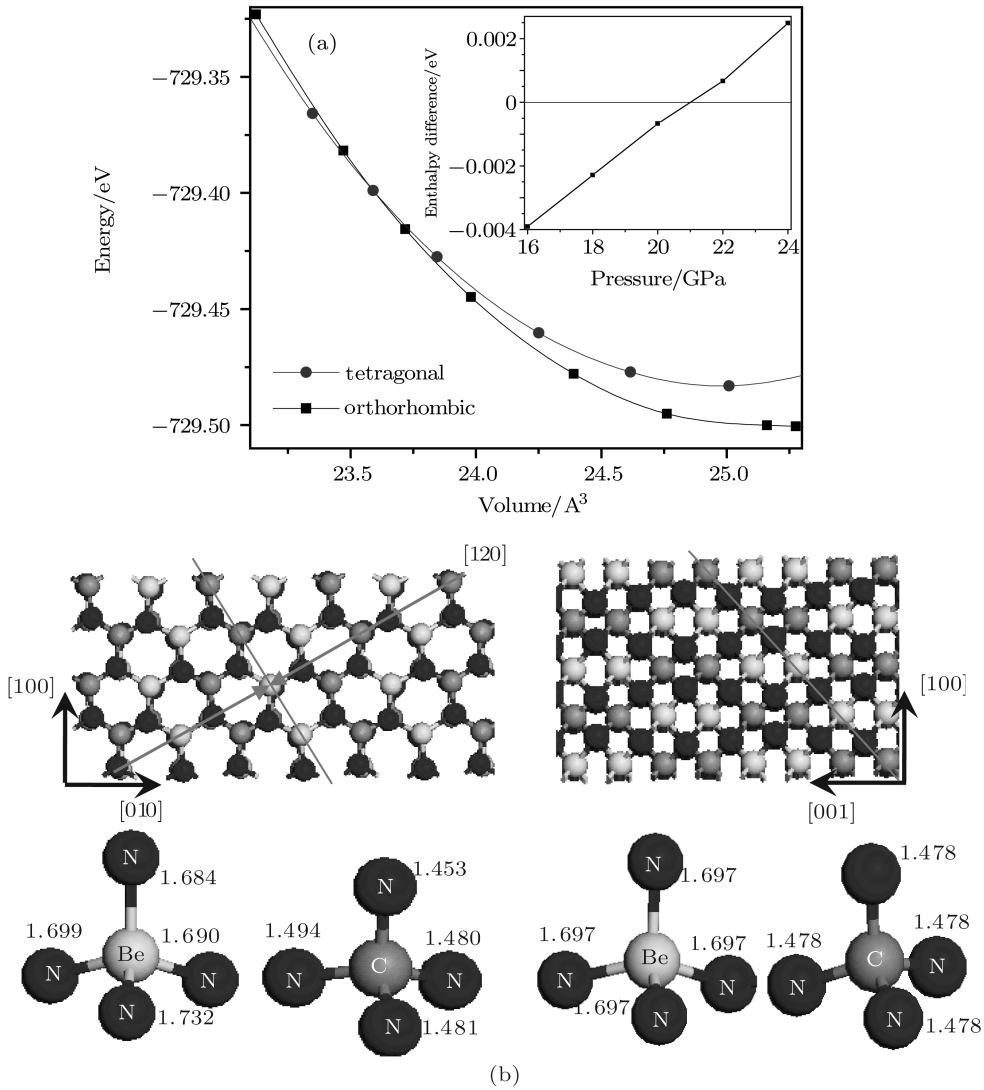


Fig. 1. (a) Total energy as a function of volume (E–V) and enthalpy difference as a function of pressure (H–P) of $BeCN_2$. (b) Transition path of $BeCN_2$ from the orthorhombic phase (left) to tetragonal phase (right) and tetrahedron subunits in these phases.

The Voigt and Reuss averages of elastic stiffness tensor $\boldsymbol{c}_{ijkl}$ can be determined by the stress tensor $\boldsymbol{\sigma}_{ij}$ and strain tensor $\boldsymbol{\varepsilon}_{kl}$ according to Hooke's law.[30] The calculated elastic constants of $BeCN_2$ in both orthorhombic and tetragonal structure are listed in Table 2 with both LDA and GGA. For both structures of $BeCN_2$, all the single elastic constants are positive and obey the usual Born–Huang stability criteria[31,32] for orthorhombic and tetragonal structures, indicating that the proposed structure of $BeCN_2$ are all mechanically stable. Moreover, the calculated phonon spectrums (see Fig. 2) display real frequencies in the entire Brillouin zone for both orthorhombic and tetragonal structure of $BeCN_2$. It suggests that both orthorhombic and tetragonal structures are thermodynamically stable for $BeCN_2$. The bulk modulus (B), shear modulus (G), Young's modulus (E), and

Poisson's ratio (v) of $BeCN_2$ phases are thus calculated and given in Table 2 according to the Voight–Reuss–Hill averaging scheme.[33] From Table 2, we notice that with LDA, C_{11} and C_{22} of orthorhombic $BeCN_2$, 747 and 682 GPa, are a little smaller than that of c-BN, 818 GPa, while C_{33} (837 GPa) of orthorhombic phase exceeds C_{11} of c-BN, this fact suggests that the resistance to linear compression in the c-axial direction of orthorhombic phase is extremely strong.[34,35] The calculated average bulk modulus (B) of orthorhombic and tetragonal $BeCN_2$, 314 and 319 GPa, respectively, are much larger than that of $BeSiN_2$ (220 and 222 GPa, respectively), which may be due to the replacement of smaller atomic radius of carbon in comparison with Si atom. The larger B of $BeCN_2$ indicates that both orthorhombic and tetragonal phases are potential low compressible materials. The average shear moduli of $BeCN_2$, 294 and 293 GPa, for orthorhombic and tetragonal structures, respectively, are clearly smaller than that of BN (409 GPa), but larger than that of SiC and BeO, 200 and 159 GPa, respectively.[36] At the same time, we find that all the elastic properties (B, G and even E) of orthorhombic and tetragonal are very similar, although there is the decrease/increase of bond length across phase transition, which may suggest the similar bonding character.

Table 2. Zero-pressure elastic constants C_{ij}/GPa, isotropic bulk modulus B/GPa, shear modulus G/GPa, Young's modulus E/GPa, and Poisson's ratio v of $BeCN_2$ and compared with available experimental data with both LDA and GGA.

$BeCN_2$		C_{11}	C_{22}	C_{33}	C_{44}	C_{55}	C_{66}	C_{12}	C_{13}	C_{23}	B	G	E	v
	LDA	747	682	837	287	255	327	164	71	97	325	300	688	0.147
$Pna2_1$	GGA	700	652	775	274	247	311	144	64	86	302	287	654	0.139
	Averg.	724	667	806	281	251	319	154	68	92	314	294	671	0.143
	LDA	647		583	393		342	110	222		331; 333[19]; 315[20]	300	691	0.152
$I\text{-}42d$														
	GGA	612		551	367		322	97	197		306	285	652	0.145
	Averg.	630		567	380		332	104	210		319	293	672	0.149

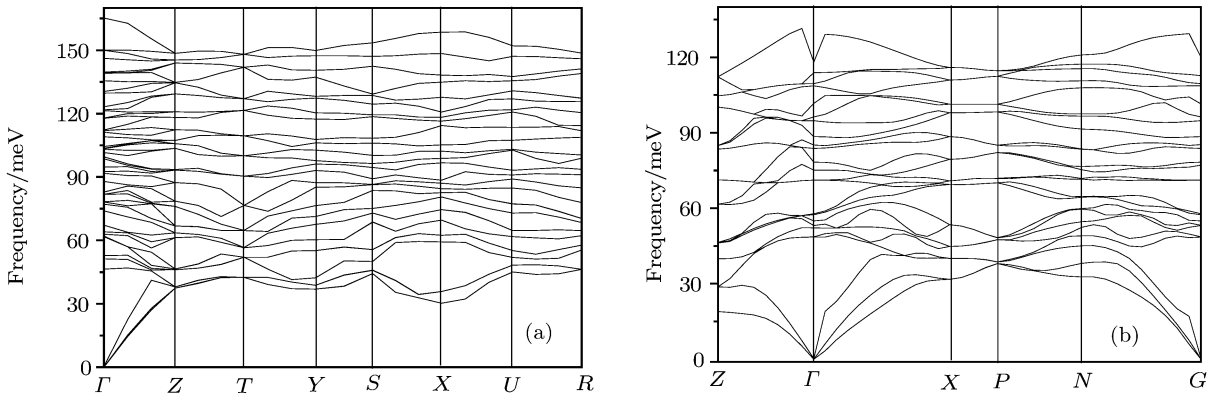


Fig. 2. Calculated phonon spectrums of $BeCN_2$ in the orthorhombic (a) and tetragonal (b) structure.

With respect to the larger bulk and shear modulus and smaller Poisson's ratio, $BeCN_2$ and even $BeSiN_2$, are expected to be potential hard materials, even superhard materials. It is known that there is no one-to-one correspondence between hardness and elastic modulus. Hardness is more complicated than the bulk modulus or shear modulus. Recently, we developed a semi-empirical model of hardness. According to the intrinsic hardness model, the weakest bond in a structure could determine the hardness of material. The Vicker hardness of $BeCN_2$ in both orthorhombic and tetragonal structures thus can be calculated as[36]

$$H_v^{\mu}(\mathrm{GPa}) = 740 P^{\mu} (v_b^{\mu})^{-5/3},$$

where P^{μ} is Mulliken overlap population of μ-type bond, v_{b}^{μ} is the volume of bond of type μ. The hardness of $MgSiN_2$ and $BeSiN_2$ are also calculated for

comparison. As shown in Table 3, the calculated hardness of $MgSiN_2$, 12.3 GPa, is close to the experimental measurement, 15 GPa,[15] indicating that the predicted hardness are reasonable. From Table 3, the calculated hardness of BeXN$_2$ (X=C, Si) in tetragonal phase are larger than that of orthorhombic ones because of the increase of Mulliken bond overlap population in the tetragonal structure. The hardness of $BeCN_2$ in tetragonal phase is 36.8 GPa, indicating an ultra-hard material, not a superhard material (larger than 40 GPa). The nanocrystalline tetragonal $BeCN_2$ phase could be a potential superhard materials.[37,38]

Table 3. The bond length of type μ, d^μ/Å^3, Mulliken bond overlap population, P^μ, the volume of bond of type μ, v_b^μ/Å^3, hardness of μ-type bond, $H^\mu_{v\mathrm{calc}}$/GPa, and hardness, $H_{v\mathrm{calc}}$/GPa, and available experimental values $H_{v\mathrm{exp}}$/GPa with LDA.

phase		bond	d^μ	P_μ	v_b^μ	$H_{v\mathrm{cal}}$	$H_{v\mathrm{expt}}$
$MgSiN_2$	$Pna2_1$	Mg–N	1.723	0.81	10.29	12.3	15[15]
$BeSiN_2$	$Pna2_1$	Be–N	1.775	0.39	4.302	25.4	
	I-42d	Be–N	1.773	0.45	4.287	29.4	
$BeCN_2$	$Pna2_1$	Be–N	1.699	0.31	3.663	26.3	
	I-42d	Be–N	1.698	0.43	3.647	36.8	

Born effective charges play a fundamental role in the dynamics of crystal lattices, which can reflect the degree of covalency or ionicity in a crystal. The calculated Born effective charges (Table 4) and high and low-frequency dielectric constants (Table 5) of $BeCN_2$ together with $BeSiN_2$ are presented by the electric field DFPT calculations in CASTEP package. Firstly, we calculated Born effective charges of c-BN, $Z^* = 1.90$, and high and low-frequency dielectric constants, $\varepsilon^\infty = 4.50$, $\varepsilon^0 = 6.77$, respectively, which are in agreement with that of the available results of $Z^* = 1.88 - 1.93$, $\varepsilon^\infty = 4.47 - 4.54$, $\varepsilon^0 = 6.79 - 7.10$,[39–43] respectively, indicating the reliability of present calculations. Crystal symmetry of BeXN$_2$ (X=C, Si) phases makes the dielectric tensors being composed of different components. The sum of all the atoms for each direction obeys the rule of charge neutrality. From Table 4, we note that the Born effective charges of all the atoms have lower values than their formal charges, +2, +4 and −3 for Be, X and N atom, respectively, and in $BeCN_2$, the deviation from their formal charges is significant, suggesting the relatively high covalent character in the bonding. The dynamical charge tensors of Be atom increase from $BeCN_2$ to $BeSiN_2$, while this trend did not observe in the similar Zn atom from $ZnSiN_2$ to $ZnGeN_2$ to $ZnSnN_2$.[13,14] Also, the dynamical charge tensors of Si atom in $BeSiN_2$ is more close to its formal charge in comparison with that of C atom in $BeCN_2$, indicating that the degree in ionicity increases from $BeCN_2$ to $BeSiN_2$, because Born effective charge, in contrast to the static charge, is a result of the covalence effect to decrease the amplitude of Z^*.[44] Nevertheless, the dynamical charge of Si in $BeSiN_2$ is similar with that of Si atom in $ZnSiN_2$ and Ge atom in $ZnGeN_2$,[13,14] suggesting the similar degree of bonding of Si (Ge)–N in these phases. Furthermore, compared with the orthorhombic BeXN$_2$ (X=C, Si) phases, Born effective charge tensors of Be atom in tetragonal ones have rather an anisotropy, such as the Born effective charge for the field along the z axis (Z^*_{zz}) is smaller than that for the field perpendicular to the x axis (Z^*_{xx}).

Table 4. Born effective charges of BeXN$_2$ (X=C, Si).

phase	atom	$Pna2_1$			I-42d		
		Z^*_{xx}	Z^*_{yy}	Z^*_{zz}	Z^*_{xx}	Z^*_{yy}	Z^*_{zz}
$BeCN_2$	Be	1.475	1.546	1.611	1.623	1.623	1.412
	C	1.953	1.912	1.903	1.896	1.896	2.154
	N_1	–1.855	–1.713	–1.710	–1.611	–1.909	–1.783
	N_2	–1.573	–1.745	–1.805	–1.909	–1.611	–1.783
$BeSiN_2$	Be	1.620	1.682	1.733	1.689	1.689	1.560
	Si	3.193	3.075	3.303	3.094	3.094	3.326
	N_1	–2.60	–2.378	–2.329	–2.342	–2.442	–2.443
	N_2	–2.214	–2.379	–2.707	–2.442	–2.342	–2.443

Table 5. High-frequency and static dielectric constants of BeXN$_2$ (X=C, Si).

	phase	$Pna2_1$			I-42d		
		ε_{xx}	ε_{yy}	ε_{zz}	ε_{xx}	ε_{yy}	ε_{zz}
ε^∞	$BeCN_2$	4.672	4.579	4.724	4.689	4.689	4.756
	$BeSiN_2$	4.411	4.375	4.560	4.464	4.464	4.487
ε^0	$BeCN_2$	6.973	6.854	7.201	7.071	7.071	7.280
	$BeSiN_2$	8.772	8.521	9.670	8.777	8.777	8.861

From Table 5, the calculated high-frequency and static dielectric constants are diagonal and have three (two) independent components for orthorhombic (tetragonal) BeXN$_2$ (X=C, Si) phases. We note that the high-frequency dielectric constants of BeXN$_2$ (X=C, Si) phases in the orthorhombic structure are smaller than those of the tetragonal structure. The high-frequency and static dielectric constants in z axis for both two structures are larger than the perpendicular one, which is also true for the previous calculated $ZnSiN_2$ and $ZnGeN_2$.[13,14]

In order to gain more insight into the structural and mechanical properties of $BeCN_2$, the calculated band structures of $BeCN_2$ with orthorhombic and tetragonal structure are displayed in Figs. 3(a) and 3(b).

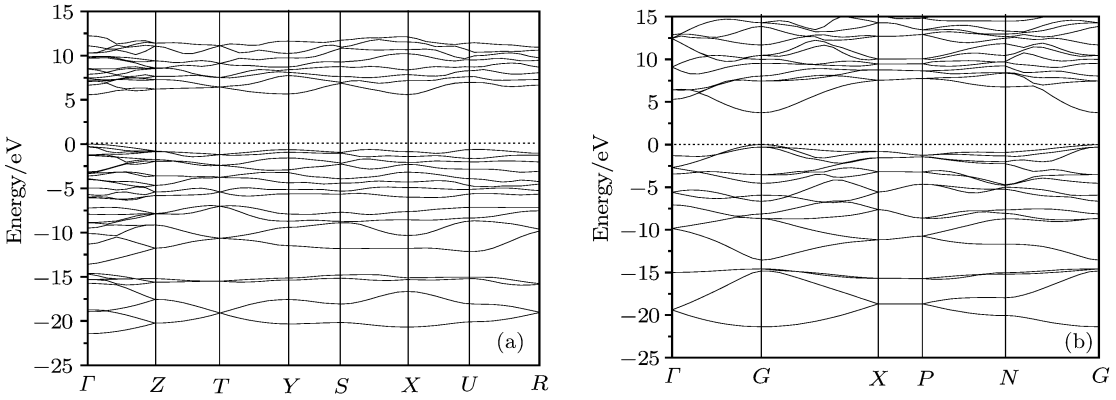


Fig. 3. Calculated band structure of $BeCN_2$ in the orthorhombic (a) and tetragonal (b) structure.

For comparison, the band structures of $BeSiN_2$ are also calculated (not shown here). The calculated band gap of orthorhombic $BeSiN_2$, 5.27 eV, is consistent with 5.19 eV of Shaposhnikov *et al.*[17] using the full potential linear augmented plane wave method. The calculated results demonstrate that both orthorhombic and tetragonal structure in $BeCN_2$ phase are semiconducting material with direct band gap of about 5.56 and 3.72 eV, respectively, located at G point. Here the calculated band gap of tetragonal structure is a little smaller than the previous calculated value (4.23 eV by Lambrecht and Segall[19] using the linear muffin tin orbital method). Nevertheless, it is known that the calculated band gaps with DFT usually underestimate by 30%–50%, the true band gap must be increased and Born effective charges and dielectric constants of BeXN$_2$ (X=C, Si) phases will be reduced correspondingly.[45,46] Moreover, we also calculate the total and partial densities of states (DOSs) of $BeCN_2$ phases shown in Figs. 4(a) and 4(b). From these figures we see that the entire DOSs show some similarity except for some detailed difference. In the lowest region the main contribution originates from the N p states and C s and p states. The valence band has a chief contribution from the p states of N and C atom and a relatively small contribution from p states of Be atom, and in this region, the covalent hybridisation between the C p states and N p states in $BeCN_2$ is always stronger than that of the Si p states and N p states in $BeSiN_2$, which is also reflected by the results of above calculated Born effective charges, i.e. $BeCN_2$ crystal is formed by the covalently bonded CN_4 and BeN_4 tetrahedron subunits, and in $BeCN_2$ crystal, the covalency of CN_4 tetrahedron is relatively stronger than that of BeN_4 tetrahedron. Moreover, the width of valence band in $BeCN_2$ phase is always larger than that of the corresponding $BeSiN_2$ phase (not shown here). The conduction band is mainly contributed by the C s and p states and Be s and p hybridisation.

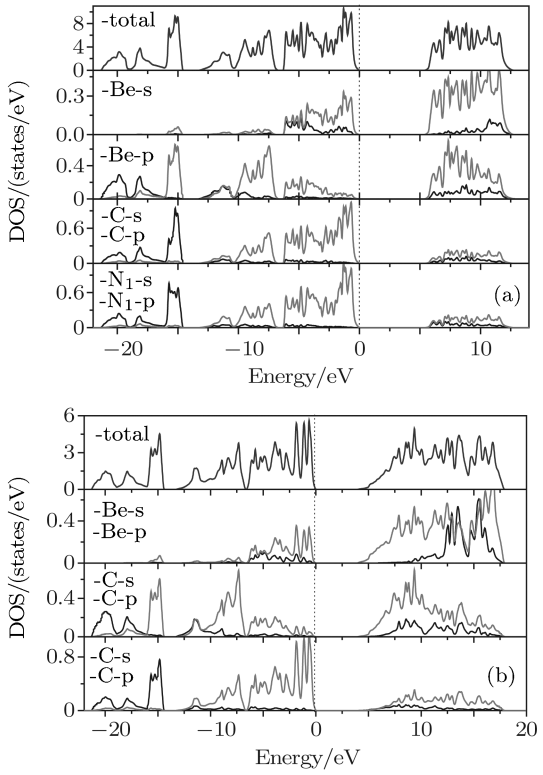


Fig. 4. Calculated total and partial DOSs of $BeCN_2$ in the orthorhombic (a) and tetragonal (b) structure.

To further understand the bonding properties of $BeCN_2$, we have given the electron density difference of both $BeCN_2$ and $BeSiN_2$ in the X–N–Be (X=C, Si) bonding planes with the orthorhombic structure as shown in Fig. 5.

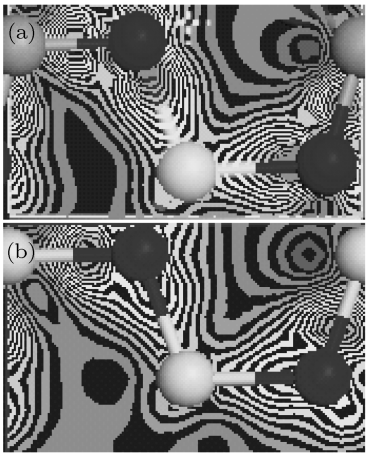


Fig. 5. Electron density difference of $BeCN_2$ (a) and $BeSiN_2$ (b) with the orthorhombic structure.

It can be seen that the electron density is localised nearby the nitrogen atom, mainly due to the p states, as discussed before. The electron density in $BeXN_2$ (X=C, Si) between X and N atom is stronger than that between Be and N atom. Furthermore, the electron density between C and N atom accumulates in the middle of bond distance of C–N, while the accumulation of electron density between Si and N atom locates at the nitrogen site slightly away from Si atom, this fact suggests a relatively high iconicity in $BeSiN_2$ phase. Moreover, by performing Mulliken population analysis, we calculate the ionic configuration to be $Be^{+0.77}N^{-0.55}C^{+0.32}N^{-0.55}$, $Be^{+0.75}N^{-0.53}C^{+0.31}N^{-0.53}$ and $Be^{+0.64}N^{-1.15}Si^{+1.65}N^{-1.15}$, $Be^{+0.61}N^{-1.12}Si^{+1.63}N^{-1.12}$ (+ and − stand for loss and gain of charge) for $BeCN_2$ and $BeSiN_2$ in orthorhombic and tetragonal structure, respectively. The results show that there are charge transfer in both $BeCN_2$ and $BeSiN_2$ phases. The charge transfers of the orthorhombic $BeCN_2$ and $BeSiN_2$ are greater than those of tetragonal $BeCN_2$ and $BeSiN_2$, respectively.

4. Conclusion

To conclude, we have investigated the structural, elastic, mechanical, dielectric and electronic properties of $BeCN_2$ in both orthorhombic and tetragonal structure by using first principle total energy calculations. The results indicate that both orthorhombic and tetragonal $BeCN_2$ phases fulfill the elastic and thermo-dynamical stability criteria. The total energy calculations indicate that the orthorhombic phases are more favourable structure under ambient condition than the tetragonal ones. Both the orthorhombic and tetragonal $BeCN_2$ phases are wide band gap materials, and the tetragonal $BeCN_2$ possesses the excellent mechanical properties. Born effective charges and dielectric constants of $BeCN_2$ also have been calculated. The electronic structure and electron density difference of $BeCN_2$ have been analysed to understand the origin of physical and bonding properties.

References

[1] Karch K and Bechstedt F 1997 *Phys. Rev.* B **56** 7404
[2] Karch K, Wagner J M and Bechstedt F 1998 *Phys. Rev.* B **57** 7043
[3] Eewin S C and Zutic I 2004 *Nature Mater.* **3** 410
[4] Mintairov A, Merz J, Osinsky A, Fuflyigin V and Zhu L D 2000 *Appl. Phys. Lett.* **76** 2517
[5] Cook B P, Everitt H O, Avrutsky I, Osinsky A, Cai A and Muth J F 2005 *Appl. Phys. Lett.* **86** 121906
[6] Parlak C and Eryigit R 2006 *Phys. Rev.* B **73** 245217
[7] Parlak C and Eryigit R 2004 *Phys. Rev.* B **70** 075210
[8] Janotti A, Wei S H, Zhang S B and Kurtz S 2001 *Phys. Rev.* B **63** 195210
[9] Jaffe J E and Zunger A 1984 *Phys. Rev.* B **30** 741
[10] Misaki T, Wakahara A, Okada H and Yoshida A 2004 *J. Cryst. Growth* **260** 125
[11] Berger T U and Schnick W 1994 *J. Alloys Comp.* **206** 179
[12] Pyykkö P 1990 *Phys. Scr.* T **33** 52
[13] Paudel T R and Lambrecht W R L 2007 *Phys. Rev.* B **76** 115205
[14] Lambrecht W R L, Alldredge E and Kim K 2005 *Phys. Rev.* B **72** 155202
[15] Groen W A, Kraan M J and With G 1993 *J. Europ. Ceram. Soc.* **12** 413
[16] Eckerlin V P 1967 *Z. Anorg. Allg. Chem.* **533** 225
[17] Shaposhnikov V L, Krivosheeva A V, Arnaud F, Lazzari J L and Borisenko V E 2007 *Phys. Stat. Sol.* B **245** 142
[18] Romer S R, Kroll P and Schnick W 2008 *J. Phys.: Condens. Matter* **21** 275407
[19] Lambrecht W R L and Segall B 1992 *Phys. Rev.* B **45** 1485
[20] Petukhov A G, Lambrecht W R L and Segall B 1994 *Phys. Rev.* B **49** 4549
[21] Kim J Y and Hughbanks T 2000 *Inorg. Chem.* **39** 3092
[22] Li L H, Li J Q and Wu L M 2008 *J. Solid State Chem.* **181** 2462
[23] Clark S J, Segall M D, Pickard C J, Hasnip P J, Probert M J, Refson K and Payne M C 2005 *Z. Krystallogr.* **220** 567
[24] Ceperley D M and Alder B J 1980 *Phys. Rev. Lett.* **45** 566
[25] Vanderbilt D 1990 *Phys. Rev.* B **41** 7892
[26] Monkhorst H J and Pack J D 1976 *Phys. Rev.* B **13** 5188
[27] Mulliken R S 1955 *J. Chem. Phys.* **23** 1833
[28] Hamann D R, Schluter M and Chiang C 1979 *Phys. Rev. Lett.* **43** 1494

[29] Refson K, Clark S J and Tulip P R 2006 *Phys. Rev.* B **73** 155114
[30] Gutiérrez G , Menéndez-Proupin E and Singh A K 2006 *J. Appl. Phys.* **99** 103504
[31] Xu H B and Wang Y X 2009 *Acta Phys. Sin.* **58** 5645 (in Chinese)
[32] Zhao W J, Xu H B and Wang Y X 2010 *Chin. Phys.* B **19** 016201
[33] Hill R 1952 *Proc. Phys. Soc. London* **65** 350
[34] Liang Y C, Li C, Guo W L and Zhang W Q 2009 *Phys. Rev.* B **79** 024111
[35] Wang H, Li Q, Li Y W, Xu Y, Cui T, Oganov A R and Ma Y M 2009 *Phys. Rev.* B **79** 132109
[36] Gao F M 2006 *Phys. Rev.* B **73** 132104
[37] Tse J S, Klug D D and Gao F M 2006 *Phys. Rev.* B **73** 140102(R)
[38] Gao F M, Tse J S and Klug D D 2007 *J. Appl. Phys.* **102** 084311
[39] Guo G Y, Ishibashi S, Tamura T and Terakura K 2007 *Phys. Rev.* B **75** 245403
[40] Gielisse P J, Mitra S S, Plendl J N, Griffis R D, Mansur L C, Marshall R and Pascoe E A 1967 *Phys. Rev.* **155** 1039
[41] Sun J, Zhou X F, Chen J, Fan Y X, Wang H T, Guo X J, He J L and Tian Y J 2006 *Phys. Rev.* B **74** 193101
[42] Ohba N, Miwa K, Nagasako N and Fukumoto A 2001 *Phys. Rev.* B **63** 115207
[43] Karch K and Bechstedt F 1997 *Phys. Rev.* B **56** 7404
[44] Ching W Y and Rulis P 2006 *Phys. Rev.* B **73** 045202
[45] Filippetti A and Spaldin N A 2003 *Phys. Rev.* B **68** 045111
[46] Pruneda J M and Artacho E 2005 *Phys. Rev.* B **72** 085107